Lattice strain pole figures analysis in titanium during uniaxial deformation

David Gloaguen, Baptiste Girault, Jamal Fajoui, Vincent Klosek, Marie José Moya

Materials Science Forum
ISSN: 1662-9752, Vol. 905, pp 74-80
doi:10.4028/www.scientific.net/MSF.905.74

Submitted: 2016-05-11
Accepted: 2017-07-17
Online: 2017-08-22

Lattice Strain Pole Figures Analysis in Titanium during Uniaxial Deformation

GLOAGUEN David[1,a*], GIRAULT Baptiste[1,b], FAJOUI Jamal[1,c], KLOSEK Vincent[2,d] and MOYA Marie-José[1,e]

[1]Université de Nantes, Institut de Recherche en Génie Civil et Mécanique, GeM (UMR CNRS 6183), 58, rue Michel Ange - BP 420, 44606 Saint-Nazaire Cedex, France

[2]CEA, IRAMIS, Laboratoire Léon Brillouin (UMR12 CEA-CNRS), CEA Saclay, 91191 Gif-sur-Yvette Cedex, France

[a]david.gloaguen@univ-nantes.fr, [b]baptiste.girault@univ-nantes.fr, [c]jamal.fajoui@univ-nantes.fr, [d]vincent.klosek@cea.fr, [e]marie-jose.moya@univ-nantes.fr

Keywords: Plasticity, strain pole figure, EPSC modelling, neutron diffraction, hexagonal material

Abstract. A theoretical and experimental study was carry out to investigate deformation mechanisms in a textured titanium alloy. *In situ* neutron diffraction measurements were performed to analyze different {hk.l} family planes ({10.0}, {10.1}, {11.0} and {00.2}) and determine the corresponding internal strain pole figures. This method was applied to a pure titanium (α-Ti) submitted to a uniaxial tensile load up to 2 %. The experimental data was then used to validate the EPSC model in order to predict the distribution of lattice strains determined by neutron diffraction for various diffraction vector directions. This comparison reveals that the model results were in good agreement with the experimental data and the simulations reproduced the lattice strain development observed on the strain pole figures determined by neutron diffraction.

Introduction

Titanium and its alloys are known to exhibit highly plastically anisotropic due to the hexagonal crystal structure. Crystal anisotropy and the role of crystallographic texture explain the development of important internal stresses/strains in a polycrystal deform plastically.

A realistic modelling of the mechanical behavior and microstructure evolution of hexagonal polycrystal can be managed thanks to crystal plasticity models such as Taylor [1] or self-consistent approaches [2-4]. This kind of models seems to be particularly well suited to describe the deformation behavior of polycrystalline metals. The internal structure of the polycrystal is introduced into the model and its evolution rules are stemmed from the governing field equations. The grain is characterized by its position and orientation and its shape defining the morphological texture. For each grain, rotations of crystalline lattices are calculated to characterize the crystallographic texture evolution. In most of the cases, each grain is considered as an entity with uniform mechanical (stress and strain) fields. Intracrystalline behavior of grains is deduced from internal variables which describe the rate of plastic glide on active slip systems according to Schmid's criterion.

The model can be validate on a specific level using the technique of lattice strain measurement by diffraction techniques. They provide the determination of lattice strains in selected grain subsets within the aggregate, as a function of the applied load. These measurements can be directly compared to model predictions of lattice (or intergranular) strains in selected grain subsets resembling the set of grains participating in a given diffraction measurement. The different material parameters (critical resolved shear stresses, hardening coefficients) can be determined by fitting the macroscopic loading curves and then, validated with neutron diffraction results.

In this study, *in situ* neutron diffraction was used to measure multiple lattice plane {hk.l} reflections and was employed to determine strain pole figures. A α-titanium submitted to a uniaxial tensile load was studied. The experimental data was used to validate the polycrystalline model in predicting the distribution of lattice strains observed by neutron diffraction in the aggregate along multiple orientations using an Euler cradle.

Self-Consistent Modelling

Plastic deformation occurs on the grain scale when the Schmid's law is verified: slip occurs on a system *g* if the resolved shear stress τ^g reaches a critical value τ_c^g (this value is call the critical resolved shear stress: CRSS) of the deformation system g. A complementary criterion states that the rate of the resolved shear stress must be equal to the incremental rate of the CRSS, i.e.:

$$\tau^g = R^g : \boldsymbol{\sigma} = \tau_c^g \text{ and } \dot{\tau}^g = \boldsymbol{R^g} : \dot{\boldsymbol{\sigma}} = \dot{\tau}_c^g . \quad (1)$$

":" denotes a contracted tensor product. $\boldsymbol{R^g}$ is the Schmid tensor on a system *g*. If $\dot{\gamma}^g$ is the rate of the plastic glide on a system *g*, the flow rule is given by:

$$\tau^g < \tau_c^g \Rightarrow \dot{\gamma}^g = 0 . \quad (2.a)$$

$$\tau^g = \tau_c^g \text{ and } \dot{\tau}^g < \dot{\tau}_c^g \Rightarrow \dot{\gamma}^g = 0 . \quad (2.b)$$

$$\tau^g = \tau_c^g \text{ and } \dot{\tau}^g = \dot{\tau}_c^g \Rightarrow \dot{\gamma}^g > 0 . \quad (2.c)$$

The critical task is to find which combination of slip systems will be really activated at each deformation step. Then, it is necessary to scan all possible combinations of potentially active slip systems to find one that satisfies the two conditions simultaneously. Computing time problems become the main task of this numerical approach. Moreover, several equivalent solutions can exist for some hardening matrix. Franz et al. [5] have proposed a different formulation to determine the slip system activity during plastic deformation. The relations (2a), (2b) and (2c) can be expressed as:

$$\dot{\gamma}^g = M^g \left(\tau^g, \tau_c^g \right) \dot{\tau}^g \quad (3)$$

The rate of the plastic glide is linked to the resolved shear stress through a function M^g.

The hardening parameter M^g can be expressed as:

$$\mathrm{M^g} = \frac{1}{\mathrm{H^{gg}}} \left[\frac{1}{2} \left(1 + \mathrm{th} \left(\mathrm{k_0} \left(\frac{\tau^g}{\tau_c^g} - 1 \right) \right) \right) \right] \left[\frac{1}{2} \left(1 + \mathrm{th} \left(\mathrm{k_0} \dot{\tau}^g \right) \right) \right] \left[\frac{1}{2} \left(1 + \mathrm{th} \left(\mathrm{k_0} \tau^g \right) \right) \right] . \quad (4)$$

$\mathrm{H^{gg}}$ is the self-hardening term. k_0 is a numerical parameter and 'th' is hyperbolic tangent function. With equation (4) and after some algebraic calculations, the constitutive response at the grain scale which links local stress and strain rates is defined by:

$$\dot{\varepsilon} = \left[\mathrm{s} + \sum_{\mathrm{g}} \left(\mathrm{R^g} : \mathrm{M^g} : \mathrm{R^g} \right) \right] : \dot{\sigma} = \ell^{-1} : \dot{\sigma} . \quad (5)$$

Where ℓ is the tangent modulus tensor defined for a grain. This tensor depends on elastic properties, stress rate, active systems and deformation history. The other mechanical properties are determined by the equations given by the Elasto-Plastic Self-Consistent (EPSC) model [2], taking into account the equations (3) and (5).

Experimental Details

For an investigation of depth-dependent stress distribution of the samples, layer removal method combined with residual stresses determination by X-ray diffraction has been employed. These experiments has been performed with a four-circle XRD 3003PTS diffractometer. The Cu-Kα radiation has been used. Electro-polishing was carried out in a solution of 90 % acetic acid and 10 % perchloric acid under a voltage of 32 V. It should be noticed that the stress relaxation during layer removal is weak because the etched surface is small (0.7 cm^2). X-ray measurements showed homogeneous residual stresses in the depth. Moreover, their values are low (< 25 MPa) and thus do not play, *a priori*, key role on the mechanical behavior.

The 6T1 four-circle (2θ, ω, φ, ψ) diffractometer at the Laboratoire Léon Brillouin (LLB, Saclay, France) was used to measure the intergranular strains during *in situ* tensile test at room temperature up to 2 % total deformation. Tensile samples with strain gauge sections of 15 × 5 × 2 mm^3 were machined along the rolling direction from the as-received sheet. A monochromatic incident wavelength of 1.159 Å has been set for the neutron measurements. *In situ* tensile test was achieved thanks to a tensile machine (MT 3000) mounted on the Eulerian cradle of 6T1 diffractometer [6].

During the *in situ* diffraction experiment, data was collected at 2 % macroscopic total strain for several specimen orientations. In this analysis, the reference $d_0(hk.l,\varphi,\psi)$ are those measured prior to the uniaxial loading The diffraction spectra were recorded with an area detector. We measured incomplete strain pole figures with φ and ψ angles ranging from 0° to 60° and 0° to 90° (Fig. 1), respectively, at both undeformed and 2 % total strain state. For each {hk.l} diffraction reflection, 49 spectra were recorded in order to determine the incomplete strain pole figure. At ψ = φ = 0°, grains with the plane normal oriented along the longitudinal direction (LD) (i.e. the loading direction) are detected (i.e. scattering vector Q aligned along LD). At ψ = 90° and φ = 0°, grains with the plane normal oriented parallel to the Transverse Direction (TD) are detected as illustrated in Fig. 1. Since the tensile testing machine is mounted perpendicularly to the sample stage, the ψ angle is defined as the angle between the normal of the selected lattice plane and the longitudinal direction. Data were collected for 4 plane families: {10.0} (2θ = 26.20°), {00.2} (2θ = 28.62°), {10.1} (2θ = 29.92°) and {11.0} (2θ = 46.23°).

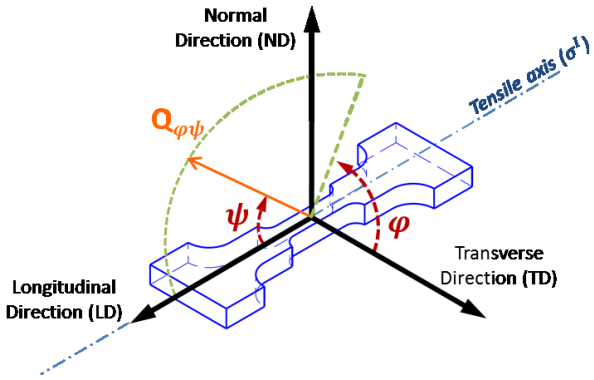

Figure 1: Orientation of the scattering vector with respect to the specimen system. Longitudinal (LD), Transverse (TD) and Normal Directions (ND) are indicated.

For each diffraction peak, $\langle \varepsilon(hk.l,\varphi,\psi)\rangle_{V_d}$ elastic lattice strain of a grain group within the diffracting volume V_d and having common {hk.l} plane-normal, parallel to the scattering vector $Q_{\varphi\psi}$, can be determined from measured interplanar spacing $\langle d(hk.l,\varphi,\psi)\rangle_{V_d}$ and a reference one $d_0(hk.l)$ for strain-free material using the following equation:

$$\langle \varepsilon(hk.l,\varphi,\psi)\rangle_{V_d} = \ln\left(\frac{\langle d(hk.l,\varphi,\psi)\rangle_{V_d}}{d_0(hk.l)}\right). \quad (6)$$

$< >_{Vd}$ indicates an averaging over diffracting grains for the considered {hk.l} reflection. d_0(hk.l) is the strain-free lattice parameter of the {hk.l} planes. $\langle d(hk.l,\varphi,\psi)\rangle_{V_d}$ is calculated using the Bragg's law once 2θ angle has been determined form diffraction peak. The strain in the scattering direction is equal to:

$$\langle \varepsilon(hk.l,\varphi,\psi)\rangle_{V_d} = ln\left(\frac{sin\,\theta_0(hk.l)}{sin\theta\,(hk.l,\varphi,\psi)}\right) \quad (7)$$

where θ_0 is the diffraction angle of the strain-free material. This reference point for calculations relates to Bragg angle measured before deformation (i.e. prior to mechanical loading) for each reflection for a given direction defined by ψ and φ angles: $\theta_0(hk.l,\varphi,\psi)$. Intergranular strains presented in this study are given as micro-strain (με, units of 10^{-6}).

The initial texture of the studied material shown in Fig. 2 was measured using neutron diffraction (6T1 diffractometer). The Orientation Distribution Function (ODF) calculation has been dug out from four independent Pole Figures (PF) ({00.2}, {10.1}, {11.0} and {10.2}) with the help of the BEARTEX program and methods described in [7]. As seen in Fig. 2, the grains are preferentially oriented with the {00.2} plane-normals ± 30° away from the Normal Direction (ND) axis (corresponding to the sheet normal direction).

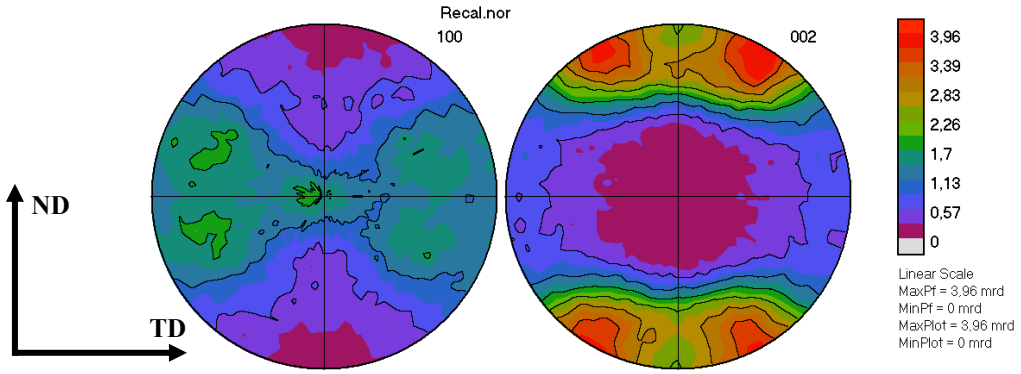

Figure 2: Initial texture ({10.0} and {00.2} PF) of α-titanium. The center of the poles is always the loading direction.

Simulation Data

During plastic deformation, the main active slip systems are assumed to be: the 6 prismatic $\{10.0\}\langle 11.0\rangle$ systems, the 24 pyramidal $\{10.1\}\langle 11.3\rangle$ systems, the 12 pyramidal $\{10.1\}\langle 11.0\rangle$ and the 6 basal $\{00.2\}\langle 11.0\rangle$. The crystallographic texture was introduced by a set of 3000 grains characterized by Euler angles and weighted by their respective volume fraction. The EPSC model takes into account a hardening law for the evolution of critical resolved shear stresses on each slip system *g* given by:

$$\dot{\tau}_c^g = \sum_h H^{gh}\dot{\gamma}^h . \quad (8)$$

where H^{gh} is the hardening matrix reflecting the different interactions between slip systems. The latent hardening coefficient are assumed to be described by a simple law. H^{gh} terms (with $g \neq h$) are taken as a fraction of the self-hardening terms H^{hh} through a constant parameters *q*: $H^{gh} = q\ H^{hh}$ ($g \neq h$) [8].

In the study, initial critical resolved shear stresses and the hardening law for slip systems are considered as controlling parameters. Their values depend on many factors (grain size, oxygen

content…) and they are unknown. They are determined comparing the predicted behavior on the experimental one (strain-stress curve and internal strains) for a tensile test. The different elastoplastic parameters corresponding to the simulations are shown in Table 1. In the present work, q is set to a value of $q = 2$ for the model calculations.

Table 1: EPSC model parameters of titanium sample.

Deformation mode	Critical resolved shear stress (CRSS) (MPa)	Self-hardening coefficient H^{gg} (MPa)
{10.0}<11.0> (pr<a>)	110	30
{00.2}<11.0> (bas <a>)	144	50
{10.1}<11.0> (pyr<a>)	168	43
{10.1}<11.3> (pyr<c+a>)	287	105

Results

Fig. 3 shows the comparison between measured and predicted stress-strain curves for the mechanical tensile test along the rolling direction. The predicted Young's modulus (107 GPa) is consistent with the experimental one (107 ± 4 GPa).

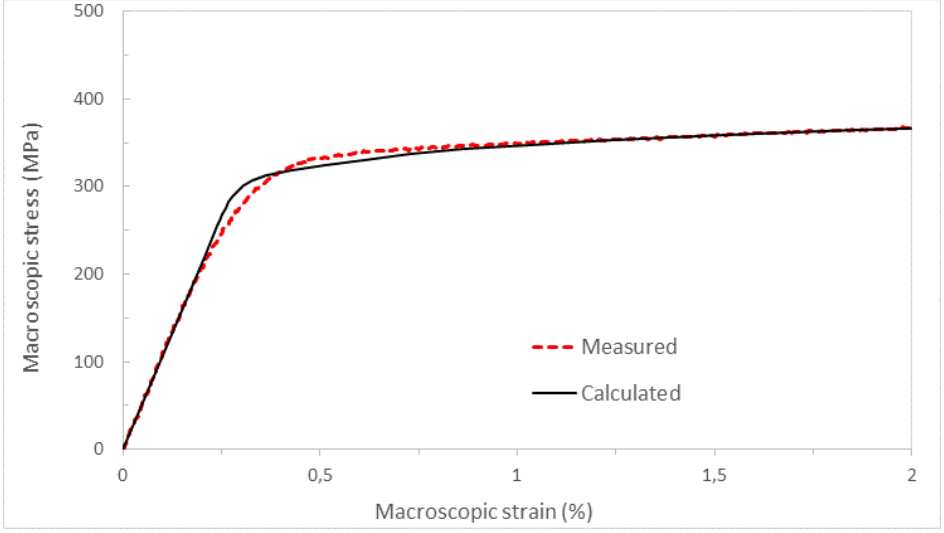

Figure 3: Experimental and predicted macroscopic stress-strain curves for α-Ti.

Fig. 4 gives the predicted relative system activities during tension along the rolling direction (or LD). It is clear that the major deformation mode is prismatic slip. The proportions of activated systems, at 2 % total strain, are: 42 % for prismatic mode, 26 % for basal slip, 22 % for pyramidal <c+a> slip and 10 % for pyramidal <a> slip.

Let's consider in more detail the development of the lattice strains for the {10.1} grains at the end of the mechanical test showed in Fig. 5. A large tensile strain develops in the longitudinal direction (i.e. loading direction) for this reflection while strain becomes more compressive as the diffraction vector Q moves toward the normal or the transverse directions. Large tensile strains ($\langle\varepsilon(10.1,0,0)\rangle_{V_d}$ = 2926 ± 183 με) near the LD (at low ψ angles) with compressive intergranular strains at high ψ angles (the minimum strain is found at ψ = 90°: $\langle\varepsilon(10.1,10,90)\rangle_{V_d}$ = -789 ± 147 με) are seen in experimental results. The intergranular strains decrease monotonically from the loading direction (LD) to the perimeter of the PF. The predicted strain PF have the same trends as the measurements, including the tensile strains along the LD and the compressive lattice strains for high ψ angles. The calculated lattice strain along the longitudinal direction (i.e. ψ = φ = 0°) for {10.1} reflection is 2960 με. A good agreement between predicted and experimental intergranular strains is obtained for this reflection. Concerning the other studied orientations defined by (φ,ψ), the EPSC approach also predicts correctly the lattice strain evolution with ψ angle. The regions of

compressive and tensile lattice strains and the decrease in internal strains with ψ value are described by the numerical simulations. For example, tensile strains are found for ψ ranging from 0° to 60° and compressive strains for 75° < ψ < 90° for the {10.1} PF. This trend is very well reproduced by the model.

Concerning the other PF not show here ({10.0}, {11.0} and {00.2}), similar quantitative agreements are also observed between predicted results and experimental data obtained with neutron diffraction technique.

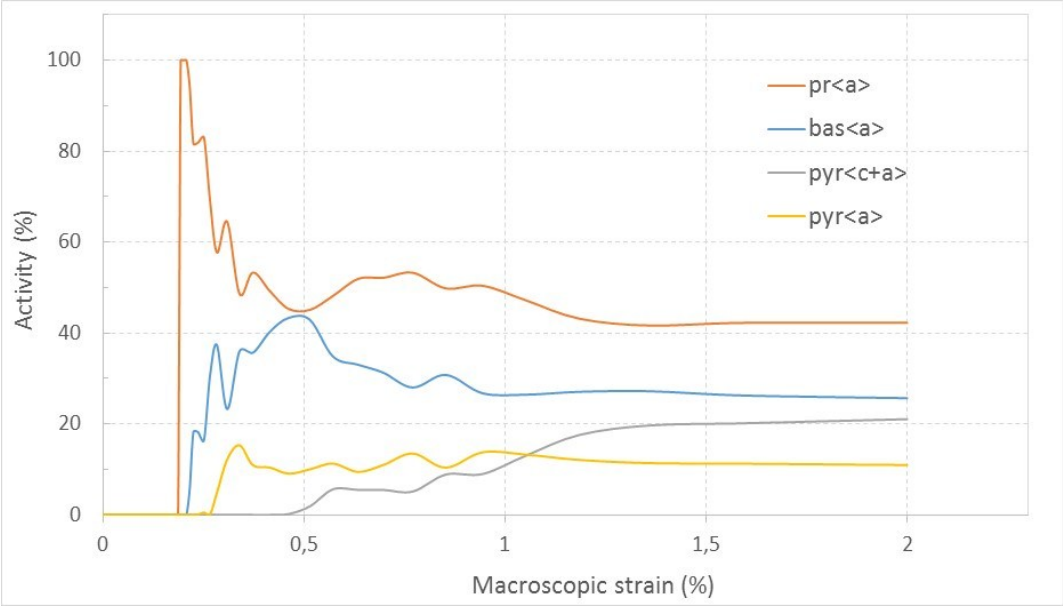

Figure 4: Relative activities of the different slip systems during the mechanical tensile test.

pr<a>: prismatic slip {10.0}⟨11.0⟩, pyr<c+a>: first-order pyramidal slip {10.1}⟨11.3⟩,pyr<a>: first-order pyramidal slip {10.1}⟨11.0⟩, bas<a>: basal slip {00.2}⟨11.0⟩.

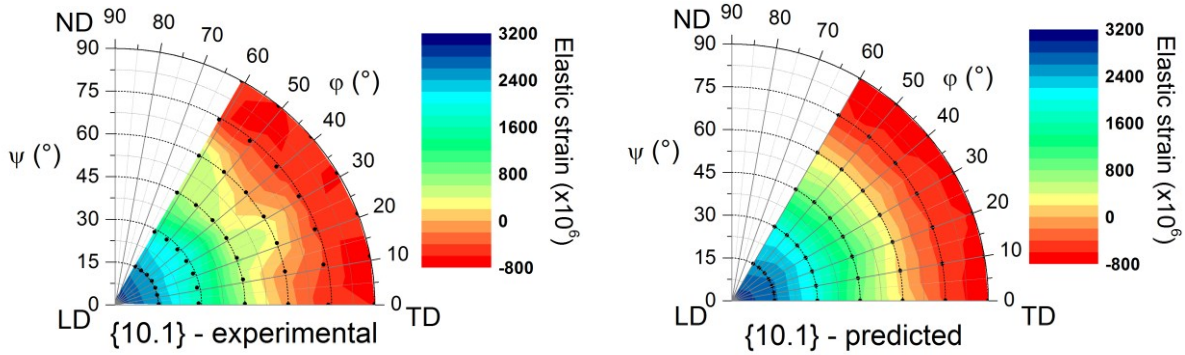

Figure 5: {10.1} lattice strain PF from neutron diffraction analysis and predicted from the self-consistent model.

Conclusions

The mechanical behavior of commercially pure titanium was studied using a scale transition model and neutron diffraction data. A modified EPSC modeling of the intergranular strain distributions at during a uniaxial tensile loading for different reflections ({10.0}, {10.1}, {11.0} and {00.2}) has been made. All model parameters (CRSS, hardening terms) were successfully determined from one simple tensile test coupled with lattice strain measurements. This was feasible because intergranular strains were measured in many (φ,ψ) directions. A combination of prismatic, basal and pyramidal <c+a> and <a> slips explains correctly the macroscopic stress-strain curve as well as the experimental strain PF for the studied reflections

References

[1] T.M. Holden, A.P. Clarke, R.A. Holt, Intergranular Stresses in Incoloy-800, J. Neutron Research. 5 (1997) 241-64.

[2] D. Gloaguen, G. Oum, V. Legrand, J. Fajoui, S. Branchu, Experimental and theoretical studies of intergranular strain in an alpha titanium alloy during plastic deformation, Acta Mater. 61 (2013) 5779-5790.

[3] B. Clausen, T. Lorentzen, A.M. Bourke, M.R. Daymond, Lattice strain evolution during uniaxial tensile loading of stainless steel, Mat. Sci. Eng. A 259 (1999) 17–24.

[4] Muransky, M.R. Barnett, V. Luzin, S. Vogel, On the correlation between deformation twinning and lüders-like deformation in a extruded Mg alloy: in situ neutron diffraction and EPSC.4 modelling, Mater. Sci. Eng. A 527 (2010) 1383-1394.

[5] G. Franz , F. Abed-Meraim, J.P. Lorrain, T. Ben Zineb, X. Lemoine, M. Berveiller, Ellipticity loss analysis for tangent moduli deduced from a large strain elastic-plastic self-consistent model, Int. J. Plasticity 25 (2009) 25-205.

[6] Information on http://www-llb.cea.fr

[7] H.R. Wenk, S. Matthies, J. Donavan, D. Chateigner, BEARTEX, a Windows-based program system for quantitative texture analysis, J. Appl. Crystallogr. 31 (1998) 262-269.

[8] D. Gloaguen, J. Fajoui, B. Girault, Residual stress fields analysis in rolled Zircaloy-4 plates: Grazing incidence diffraction and elastoplastic self-consistent model, Acta Mater. 71 (2014) 136-144.